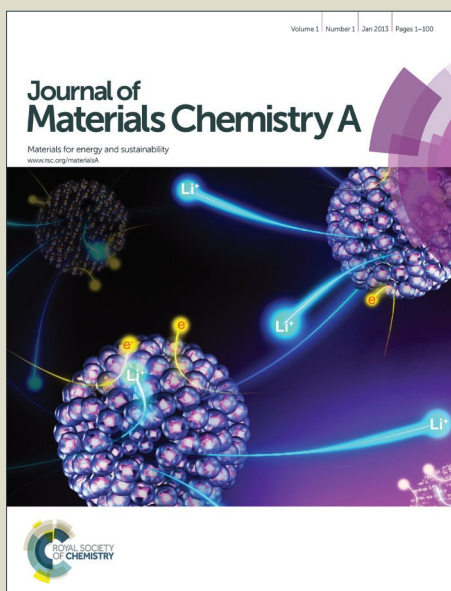


Journal of Materials Chemistry A

Accepted Manuscript



This is an *Accepted Manuscript*, which has been through the Royal Society of Chemistry peer review process and has been accepted for publication.

Accepted Manuscripts are published online shortly after acceptance, before technical editing, formatting and proof reading. Using this free service, authors can make their results available to the community, in citable form, before we publish the edited article. We will replace this *Accepted Manuscript* with the edited and formatted *Advance Article* as soon as it is available.

You can find more information about *Accepted Manuscripts* in the [Information for Authors](#).

Please note that technical editing may introduce minor changes to the text and/or graphics, which may alter content. The journal's standard [Terms & Conditions](#) and the [Ethical guidelines](#) still apply. In no event shall the Royal Society of Chemistry be held responsible for any errors or omissions in this *Accepted Manuscript* or any consequences arising from the use of any information it contains.



Journal Name

ARTICLE IN PRESS

Visible-light sensitive Cu(II)-TiO₂ with sustained anti-viral activity for efficient indoor environmental remediation

Min Liu,^b Kayano Sunada,^b Kazuhito Hashimoto,^{*bc} Masahiro Miyauchi^{*ad}

Received 00th January 20xx,
Accepted 00th January 20xx

DOI: 10.1039/x0xx00000x

www.rsc.org/

Visible-light sensitive photocatalysts are desirable for indoor environmental remediation applications. Photocatalysts used for indoor environmental applications must have efficient visible-light activity and sustainable function in dark conditions, as indoor light apparatuses are typically switched off during the night. Herein, we report the synthesis and optimization of a highly visible-light sensitive Cu(II)-TiO₂ nanocomposite with sustained anti-viral activity in dark conditions. The synthesized Cu(II)-TiO₂ exhibited superior volatile organic compound decomposition and anti-viral activity under visible-light irradiation. Its quantum efficiency for the decomposition of gaseous 2-propanol reached 68.7%. In addition, Cu(II)-TiO₂ completely inactivated bacteriophage within 30 min of visible-light irradiation. Notably, the Cu(II)-TiO₂ photocatalyst also exhibited sustained anti-viral activity in dark conditions after visible-light irradiation treatment. Taken together, these findings indicated that the prepared Cu(II)-TiO₂ is potentially an effective risk-reduction material for indoor applications.

1. Introduction

Indoor air quality is an important health and safety factor due to its influences on population health and wellbeing.^{1,2} The air levels of volatile organic compounds (VOCs) are of particular concern because these harmful chemicals cause a wide range of human health problems, including sick house syndrome.³ Infectious pathogens are also frequently encountered in our daily environment and can adversely impact human health.^{4,5} As a promising solution for environmental remediation, photocatalytic oxidation using semiconductors has attracted considerable attention. However, because most efficient photocatalysts are wide band-gap semiconductors, such as TiO₂, which are only activated by ultraviolet (UV) light irradiation, they have been limited to outdoor applications.⁶⁻⁹ As indoor light sources contains low levels (below several μW/cm² in white light fluorescent light)¹⁰ or no UV light (white incandescent light and white light emission diodes [LEDs]), it is highly desirable to develop visible-light-sensitive photocatalysts for indoor environmental purification applications.

Over the past few decades, attempts to develop visible-

light-sensitive photocatalysts have focused on the doping of TiO₂ with various transition metal ions or anions. Despite these efforts, most systems are not suitable for practical indoor applications because of their low quantum efficiencies (QEs) caused by the carrier recombination centers in metal-ion-doped TiO₂ or the low oxidation power and mobility of photogenerated holes in non-metal-doped TiO₂.¹¹⁻¹³ As an alternative strategy to doping, our group previously demonstrated that the surface modification of TiO₂ with Cu(II) or Fe(III) nanoclusters increases the visible-light-sensitivity of the resulted material without inducing impurity levels in the band gap.¹⁴⁻¹⁹ In the case of Cu(II) nanocluster-grafted TiO₂ (Cu(II)-TiO₂), electrons in the valence band (VB) of TiO₂ are excited to the Cu(II) nanoclusters under visible-light irradiation through an interfacial charge transfer (IFCT) process. The introduction of excited electrons into the Cu(II) nanoclusters leads to the formation of Cu(I) species, which efficiently reduce oxygen molecules. During the IFCT process, holes with strong oxidative power for the decomposition of organic compounds are generated in the deep VB of TiO₂.¹⁹ Thus, nanocluster-modified TiO₂ is a promising material for visible-light-sensitive photocatalytic applications.

Practical photocatalytic systems for indoor environmental remediation require the following characteristics: (i) composed of robust inorganic materials that are nontoxic and derived from naturally abundant elements; (ii) visible-light sensitivity with strong oxidation power; and (iii) anti-pathogenic (antibacterial and antiviral) effects, even in dark conditions. Cu(II) or Fe(III) nanocluster-grafted TiO₂ satisfy the first requirement, as they consist of non-toxic and earth-abundant elements.²⁰⁻²² Regarding visible-light sensitivity, the reaction rate and QE of Cu(II)-grafted TiO₂ are reportedly lower than those of Fe(III)-grafted TiO₂.¹³⁻¹⁶ For the third requirement,

^a Department of Metallurgy and Ceramics Science, Graduate School of Science and Engineering, Tokyo Institute of Technology, 2-12-1 Ookayama, Meguro-ku, Tokyo 152-8552, Japan. E-mail: mmiyauchi@ceram.titech.ac.jp

^b Research Center for Advanced Science and Technology, The University of Tokyo, 4-6-1 Komaba, Meguro-ku, Tokyo 153-8904, Japan. E-mail: hashimoto@light.l.u-tokyo.ac.jp

^c Graduate School of Engineering, The University of Tokyo, 7-3-1 Hongo, Bunkyo-ku, Tokyo 113-8656, Japan.

^d Japan Science and Technology Agency (JST), 4-1-8 Honcho Kawaguchi, Saitama 332-0012, Japan.

† Electronic Supplementary Information (ESI) available: ICP, XPS, XRD, SEM, UV-Vis, photocatalytic performance measurements and calculated photocatalytic performances for Cu(II)-TiO₂ samples. See DOI: 10.1039/x0xx00000x

copper oxides, particularly copper monoxide, is reported to have strong anti-viral activity, even under dark conditions,²⁰⁻²³ as compared to iron-based oxides. Therefore, the optimization and improvement of Cu(II)-TiO₂, particularly with respect to increasing the visible-light activity and sustained anti-viral function of Cu(II) nanocluster-modified TiO₂ are key challenges for developing efficient indoor applications for environmental remediation.

In this work, we comprehensively optimized the synthesis conditions for grafting Cu(II) nanoclusters onto TiO₂ to increase the reaction rate and QE of this photocatalyst. In addition to achieving the highest visible-light activity among reported Cu(II)-TiO₂ photocatalysts, we demonstrated that Cu(II)-TiO₂ has sustained anti-viral activity, even under dark conditions after visible-light irradiation. Irradiation of Cu(II)-TiO₂ with visible light cause the Cu(I) species to reach an excited state, which critical for the anti-viral function in both light and dark conditions. The Cu(II)-TiO₂ material is photocatalytically activated by indoor light irradiation and also maintains the anti-viral activity under dark conditions. Due to these properties, the presently synthesized Cu(II)-TiO₂ photocatalyst has great potential as an effective material for indoor purification applications aimed at minimizing risks to private and public health.

2. Experimental section

2.1 Synthesis of Cu(II)-TiO₂ Samples. Cu(II)-TiO₂ samples were prepared using a modified impregnation method, as described previously (19). Briefly, commercial TiO₂ (MT-150A, Tayca Co.; rutile phase, 15-nm grain size, 90 m²/g specific surface area) was annealed at 950 °C for 3 h. The calcined TiO₂ was treated with a 6 M HCl aqueous solution at 90 °C for 3 h under continuous stirring. After passing the reaction mixture through a membrane filter (0.025 μm, Millipore), the products were collected and then washed thoroughly with distilled water. The obtained TiO₂ powder was dried at 110 °C for 24 h and was then ground into a fine powder using an agate mortar and pestle. For the grafting of Cu(II) nanoclusters, 1 g TiO₂ powder was dispersed in 10 mL distilled water, to which copper chloride dihydrate (CuCl₂·2H₂O, Wako, 99.9%) was then added. The weight fraction of Cu relative to TiO₂ was set to 0.1% and the pH value of the solution was adjusted to 12 using sodium hydroxide (NaOH). The resulting suspension was heated at 90 °C under continuous stirring for 1 h in a vial reactor. The obtained product was filtered through a 0.025-μm membrane filter (Millipore) and then washed with sufficient amounts of distilled water. Finally, the obtained product (denoted as Cu(II)-TiO₂ (950-HCl-12)) was dried at 110 °C for 24 h and was subsequently ground into a fine powder using an agate mortar and pestle. The above-mentioned procedure is the typical synthesis condition used to achieve the optimum photocatalytic activity of Cu(II)-TiO₂ and was determined by evaluating the following parameters: temperature of annealing on TiO₂ powder, aqueous HCl treatment to clean the TiO₂ surface, pH value for Cu(II) grafting, and amount of Cu(II) ions in aqueous solution.

2.2 Sample characterization. The crystal structures of the prepared Cu(II)-TiO₂ nanocomposites were measured by powder X-ray diffraction (XRD) at room temperature on a Rigaku D/MAX25000 diffractometer with a copper target ($\lambda = 1.54056 \text{ \AA}$). Elemental analyses of the samples were performed using an inductively coupled plasma-atomic emission spectrometer (ICPAES; P-4010, Hitachi). UV-visible absorption spectra were recorded by the diffuse reflection method using a UV-2550 spectrometer (Shimadzu). The morphologies of the prepared TiO₂ nanocomposites were investigated by scanning electron microscopy (SEM) using a Hitachi SU-8000 apparatus and transmission electron microscopy (TEM) using a Hitachi HF-2000 instrument with an acceleration voltage of 200 kV. The specific surface areas of the samples were determined from nitrogen absorption data at liquid nitrogen temperature using the Barrett-Emmett-Teller (BET) technique.²⁴ Briefly, the samples were degassed at 200 °C and the pressure was kept below 100 mTorr using a Micromeritics VacPrep 061 instrument for a minimum of 2 h prior to the analysis. Surface compositions were studied by X-ray photoelectron spectroscopy (XPS; model 5600, Perkin-Elmer). The binding energy data were calibrated with reference to the C 1s signal at 284.5 eV. The thermogravimetric analysis of the samples was performed using a Rigaku Thermo plus TG 8120 apparatus with a temperature range between 298 and 1473 K in air atmosphere and at a heating rate of 10 °C/min.

2.3 Evaluation of photocatalytic properties. The decomposition of gaseous (2-propanol) IPA in air atmosphere was chosen as a probe to evaluate the photocatalytic activities of the samples. For the analysis, 0.3 g powder samples were evenly dispersed on the bottom of a circular glass dish (5.5 cm²), which was set in the center of a 500-mL cylindrical glass vessel reactor. After the vessel was sealed with a rubber O-ring and a quartz cover, the reactor was evacuated and filled with fresh synthetic air. To avoid organic contamination of the sample surface, the vessel was pre-illuminated with an Xe lamp (Luminar Ace 210, Hayashi Tokei Works) until the CO₂ generation rate was less than 0.02 μmol/day. The vessel was re-evacuated and re-filled with fresh synthetic air, and the internal pressure was maintained at approximately 1 atm. To begin the decomposition analysis, 300 ppm of gaseous IPA was injected into the vessel. Prior to light irradiation, the vessel was kept in the dark for a sufficient time (approximately 12 h) to achieve absorption/desorption equilibrium of IPA on the photocatalyst surface. The vessel was then irradiated by visible light with wavelengths from 420 to 530 nm emitted from an Xe lamp equipped with a combination of glass filters (B-47, L-42, and C-40C; AGC Techno Glass). The light intensity was measured using a spectroradiometer (USR-40D, Ushio) and was set to 1 mW/cm². During the light irradiation, 1 mL gaseous samples were periodically extracted from the reaction vessel to detect the concentrations of IPA, acetone and CO₂ using a gas chromatograph (model GC-8A, Shimadzu Co., Ltd.).

2.4 Evaluation of anti-viral activity. Cu(II)-TiO₂ was coated on a glass substrate (2.5 cm × 2.5 cm) by simply drop casting 150 μL of an ethanol suspension of Cu(II)-TiO₂ (1 mg/mL). The total

amount of Cu(II)-TiO₂ coated on the substrate was 0.3 mg/6.25 cm², which is equal to 0.48 g/m². The glass surface was dried and then sterilized at 120 °C for 3 h. Q β bacteriophage (NBRC 20012) and *Escherichia coli* (NBRC 13965) as the host bacterium were used in the evaluation experiment. A stock suspension of Q β bacteriophage ($\sim 1.2 \times 10^{11}$ plaque forming units per mL [PFU/mL]) was used to infect *E. coli* cells at 35 °C for 10 min, and then was plated onto a double-layered medium, which was prepared with Nutrient broth (Difco) and agar (Difco) by adjusting the agar concentration of the bottom layer to 1.5% and that of the top layer to 0.5%. The plates were then further incubated overnight at 35 °C, and the top agar layer containing the cells and bacteriophage was then collected and added to 2 mL/plate SM buffer (0.1 M NaCl, 8 mM MgSO₄, 50 mM Tris-HCl [pH 7.5] and 0.1% gelatin) at 4 °C for overnight. The solution was centrifuged (8000 \times g, 4 °C, 20 min) and the resulting supernatant containing bacteriophage was collected and filtered (0.22 μ m, Millipore, MA). The bacteriophage solution was diluted with PBS to give approximately 2.5×10^9 PFU/mL, and 50 μ L of the diluted suspension was then pipetted onto the Cu(II)-TiO₂ coated glass. The glass samples were irradiated using 10-W white light bulbs at an illuminance of 1000 lux. The light illuminance was measured using an illuminance meter (IM-5, Topcon), and irradiation with visible light with wavelengths above 400 nm was performed using a white fluorescence light bulb through a UV cutoff film. After irradiation, the bacteriophage suspension was collected into SM buffer (10 mL). An appropriate dilution of the collected suspension was used to infect *E. coli* cells, which were then plated onto Nutrient agar medium using the above-described double-layer method to determine the number of plaques.

3. Results and discussion

3.1 Improvement of visible-light sensitivity of Cu(II)-TiO₂.

To improve the visible-light activity of Cu(II)-TiO₂, we investigated the effect of the synthesis conditions, including the pre-annealing treatment of bare TiO₂ powder, washing treatment of TiO₂ in aqueous acid conditions, pH during the grafting of Cu(II) nanoclusters, and amount of Cu(II) nanoclusters, on the photocatalytic activity. To investigate the effect of the pre-annealing conditions for TiO₂ powder, XRD patterns of TiO₂ powder annealed for 3 h at temperatures ranging from 300 to 1150 °C were measured (Figure 1a). TG-DTA analysis was also performed and revealed that endothermic and exothermic peaks of the TiO₂ powder appeared at approximately 440 and 935 °C, respectively (Supplementary Information, Figure S1). The endothermic peak mainly originated from the removal of surface-absorbed compounds,²⁵ which resulted in a decrease of the powder weight between 400 and 500 °C. The exothermic peak was attributed to the crystallization of the powder,²⁵ indicating that the TiO₂ powder obtained at approximately 935 °C possessed good crystallinity. The XRD patterns of the annealed powders showed that all of the samples had a rutile structure (JCPDS card no. 21-1276). In addition, the diffraction peaks

became sharper with increasing annealing temperature, indicating that the crystallinity of the samples was improved by the annealing treatment. Figure 1b shows the influence of the pre-annealing temperature on the specific surface area and

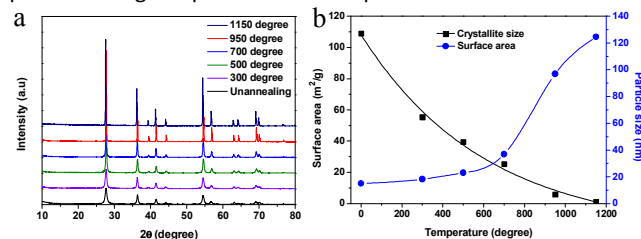


Figure 1. (a) XRD patterns for TiO₂ samples obtained at various annealing temperatures, and (b) crystallite sizes and surface areas of TiO₂ versus annealing temperature.

crystallite size of TiO₂, as determined by Scherrer's equation.²⁶ The annealing treatment resulted in an increase in the crystallite size of the TiO₂ powder (from ~ 15 to ~ 125 nm), but markedly decreased the total surface area. SEM image analysis clearly showed that the particle size increased with increasing annealing temperature (Figure S2). Notably, performing the annealing step at over 950 °C resulted in significant crystal growth and caused the color of the powder to change from white to brown (Figure S3), indicating the introduction of oxygen defects or generation of Ti³⁺ species in the sample.¹⁷ Oxygen defects or Ti³⁺ species have been demonstrated to reduce the photocatalytic performance of TiO₂.¹⁷ Further, the surface areas of the samples obtained at 950 and 1150 °C were ~ 5.8 and ~ 1.2 m²/g, respectively, which are markedly smaller than the ~ 110 m²/g area of the starting TiO₂ powders.

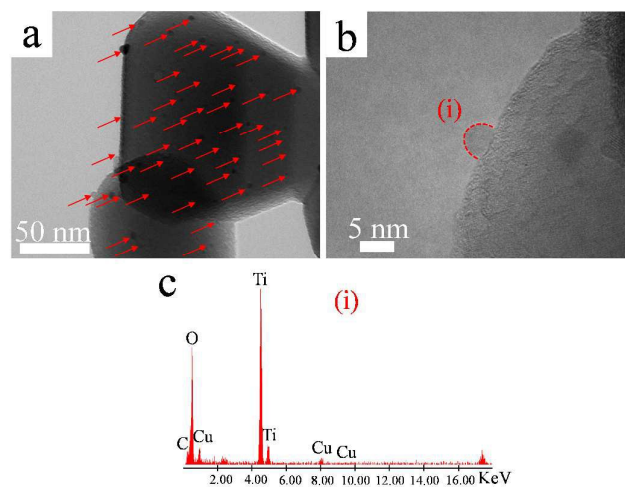


Figure 2. a) TEM and b) HRTEM images of Cu(II)-TiO₂ (950-HCl-12). Nanoclusters (indicated by red arrows) were highly dispersed on the TiO₂ surface. In b), the short dashed curve outlines a single Cu(II) nanocluster. The good attachment of nanoclusters and TiO₂ can be clearly observed. c) EDS point analysis of Cu(II) nanocluster on the point (i) in panel b).

Figure 2 shows the TEM and energy-dispersive X-ray spectroscopy (EDS) analyses of the Cu(II)-TiO₂ (950-HCl-12) sample, which was prepared by pre-annealing TiO₂ at 950 °C, acid treating before Cu(II) grafting, and grafting the Cu(II)

clusters under pH 12 conditions. These conditions were determined to result in optimal photocatalytic activity of the prepared material, as described in detail below. The TEM analysis revealed that Cu(II) nanoclusters were well dispersed

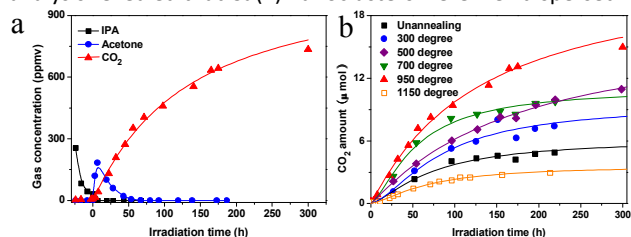


Figure 3 a) Representative time-dependent gas concentrations during IPA decomposition by the Cu(II)-TiO₂ (950-7) sample under visible-light irradiation. b) Comparative analysis of CO₂ generation by Cu(II)-TiO₂ synthesized at different temperatures under the same conditions.

on the surface of TiO₂ (Figure 2a). High-resolution TEM (HRTEM) image analysis showed that the Cu(II) nanoclusters were ~3 nm in size and well attached to the TiO₂ surface (Figure 2b). EDS point analysis (Figure 2c) revealed that the nanoclusters were composed of Cu. We also measured the XPS spectra for the Cu(II)-TiO₂ (950-HCl-12) sample (Figure S4) and confirmed that Cu(II) species were present on the TiO₂ surface. The optical absorption properties of Cu(II)-TiO₂ and bare TiO₂ were recorded and are shown in the Supplementary Information (Figure S5). For bare TiO₂, no absorption was observed in the UV-Vis spectra at wavelengths shorter than 420 nm other than the band-gap excitation of rutile TiO₂. However, after the grafting of Cu(II) nanoclusters on the TiO₂ surface, new absorptions in the regions of 420-550 and 700-800 nm were observed (Figure S5). The slight increase in absorption in the former region was attributed to the IFCT process of VB electrons to surface Cu(II) nanoclusters, whereas the increase in the latter region was assigned to a simple d-d transition of Cu(II).¹⁴

The photocatalytic activity of the Cu(II)-TiO₂ samples was evaluated by the visible-light-induced oxidation of IPA, which is frequently used as a representative gaseous VOC and is a harmful indoor air pollutant.²⁷ The photocatalytic oxidative decomposition of IPA proceeds via the formation of acetone as an intermediate, followed by the further decomposition of acetone to the final products CO₂ and H₂O (Figure 3a).²⁸ During the photocatalytic tests, the light intensity was adjusted to ~1 mW cm⁻², which corresponds to an illuminance of ~300 lux and is comparable to the intensity of typical indoor fluorescent and LED lights. The wavelength of the irradiation light ranged from 420 to 530 nm, and the initial IPA concentration was set to 300 ppmv (~6 μmol). For all samples shown in Figure 3, Cu(II) nanoclusters were grafted at pH 7. The photocatalytic performance of the TiO₂ samples increased with increasing annealing temperature up to 950 °C (Figure 3b). The performance of the TiO₂ sample obtained at an annealing temperature of 950 °C was markedly higher than that of the un-annealed sample. The QE was determined by the reaction rate (*R*) and number of absorbed photons (Figure S6). For the sample prepared by pre-annealing treatment at 950 °C, the QE

was 13.2%. However, when the annealing temperature exceeded 950 °C, the photocatalytic activity of the samples markedly decreased. These results are attributable to the formation of oxygen or Ti³⁺ defects at high temperature. Thus, the sample obtained at 1150 °C exhibited the lowest photocatalytic performance. This finding indicates that TiO₂ with good crystallinity and few defects, meaning less recombination centers, is important for the photocatalytic activity of the Cu(II)-TiO₂ system, even though the TiO₂ surface area is significantly decreased. In addition to crystallinity, aqueous acid treatment of the TiO₂ powder prior to the grafting of Cu(II) clusters is critical for the removal surface contaminants and achieving high photocatalytic performance. Previous studies have reported that the presence of contaminants, such as alkali and alkali earth elements (Na⁺ or Ca²⁺), markedly deteriorates the photocatalytic activity of TiO₂.^{29,30} The present XPS spectra analysis revealed that surface contaminants, including Na⁺ and Ca²⁺, were removed by acid treatment in hydrochloric acid (HCl) solution (Figure S7). Owing to the high acid stability of TiO₂, there is no obvious difference could be observed in the morphologies of the TiO₂ samples with or without acid treatment (Figure S8). Thus, the QE value for Cu(II)-TiO₂ was improved from 13.2 % to 30.3 % by acid treatment (950-HCl-7 in Table 1), since the surface contaminant was removed by acid treatment, resulting efficient charge transfer between TiO₂ and Cu(II) clusters.

In the above experiment, Cu(II) grafting was performed under neutral pH conditions. To examine the effect of pH during grafting on the photocatalytic activity of Cu(II)-TiO₂, we next attempted to optimize the pH of the solution used for the grafting of Cu(II) nanoclusters. We used the TiO₂ powder prepared using a pre-annealing temperature of 950 °C and HCl treatment as a starting material. From the UV-Vis spectra of the Cu(II)-TiO₂ samples prepared at different pH values, it can be seen that visible-light absorption caused by either the IFCT process or the d-d transition of Cu(II) was increased with increasing alkalinity (Figure 4a). The increase of the d-d transition of Cu(II) indicates that the amount of Cu(II) in the samples had increased in the samples prepared at higher pH, a finding that was confirmed by XPS and ICP measurements (Figure S9 and Table S1). At pH values below 12, only a limited amount of Cu(II) nanoclusters (less than 20% of added CuCl₂ salt in aqueous solution) was grafted on the TiO₂ surface. In contrast, when the pH value was above 12, nearly all Cu(II) ions in solution were grafted onto the TiO₂ surface as nanoclusters. Thus, the IFCT visible-light absorption was sharply increased at pH values over 12 (Figure 4a, inset). The observed influence of the pH on the amount of grafted Cu(II) nanoclusters may be due to the dependence of the surface charge of TiO₂ on pH. In strong acid (HCl) conditions, the TiO₂ surface is charged positive, as the pH value of the isoelectric point of bare TiO₂ is neutral at a pH of approximately 6.³¹ Therefore, high pH conditions cause a negative shift in the surface TiO₂ charge, allowing for the efficient grafting of Cu(II) clusters. It is noted that we could not see the obvious loading amount dependence on photocatalytic activities, when the pH condition was neutral (Figure S10). These results also imply

that the TiO₂ surface is positive charged after the acid treatment, then the amount of loaded Cu(II) nanoclusters strongly depends on the initial Cu(II) concentration. It is also possible that the dependence of the Cu(II) nanocluster grafting efficiency on pH is due to the hydrolysis of Cu(II) ions. Cu(II) ions are poorly soluble in highly alkaline solutions and precipitate as black-brownish CuO particles, as shown in Figure S11. In the present study, when the pH value of Cu(II) solution was increased to 14, we confirmed that CuO crystals were formed (Figure S12). Our group previously demonstrated that bulk crystal CuO particles poorly consume photogenerated electrons,¹⁹ which is crucial for the IFCT process and the multi-electron reduction reaction. At pH values below 12, the heterogeneous hydrolysis of Cu(II) ions occurs on the surface of TiO₂ powder, resulting in a good junction between the Cu(II) nanoclusters and TiO₂ surface. In the present experimental conditions, a pH value of 12 was

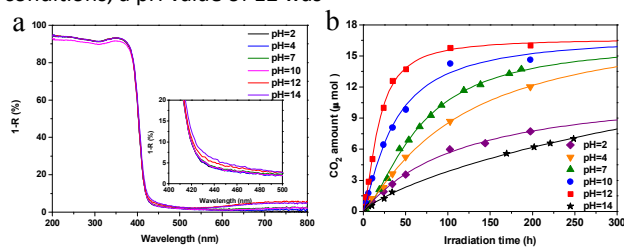


Figure 4 (a) UV-Vis spectra for Cu(II)-TiO₂ (950-HCl) samples prepared at different pH values. (b) CO₂ generation curves for the prepared samples under visible-light irradiation.

optimal for the grafting Cu(II) nanoclusters. Further, XPS spectra showed that the chemical states of elemental Ti and O were similar in Cu(II)-TiO₂ prepared at pH 12 and bare TiO₂ (Figure S13). Taken together, the results indicate that the chemical state and environment surrounding the Cu(II) nanoclusters in the Cu(II)-TiO₂ sample prepared at pH 12 were highly similar to those of a previously characterized Cu(II)-TiO₂ system.^{14,19}

Figure 4b shows the photocatalytic performances of the Cu(II)-TiO₂ (950-HCl) samples prepared at different pH values. It can be seen that the photocatalytic activity of Cu(II)-TiO₂ increased with increasing pH during the grafting of Cu(II) nanoclusters. The limited photocatalytic performance of the samples prepared at pH values less than 12 is likely attributable to the limited amount of Cu(II) nanoclusters on the positively charged TiO₂ surface. As the pH increased, the TiO₂ surface became more negative, and the amount of surface-grafted Cu(II) nanoclusters increased, leading to a corresponding increase in the photocatalytic activity of Cu(II)-TiO₂. Notably, the sample exhibited the highest performance at a pH of 12. The calculated QE and R for this sample were 68.7% and 0.40 μmol/h, respectively (Table 1), which are the highest values reported to date for a Cu(II)-TiO₂ photocatalytic system.^{14,17,19,21,22} A further increase in the pH value resulted in a drastic decrease of the photocatalytic performance, because the Cu(II) nanoclusters were changed into CuO crystals, leading to a marked decrease in the multi-electron reduction reaction

rate and the reduced consumption of photogenerated electrons.¹⁹

We also attempted to optimize the amount of Cu(II) grafted on the TiO₂ surface at pH 12 (Figure 5). ICP measurements showed that nearly all of the Cu(II) was grafted on the surface of TiO₂ at pH 12 and that the total amount of grafted Cu(II) increased with increasing levels of the initial Cu(II) concentration (Table S2). Consistent with this finding, the visible-light absorption of the Cu(II)-TiO₂ samples increased with increasing amount of grafted Cu(II) (Figure 5a). Measurement of the photocatalytic performances of the Cu(II)-TiO₂ samples showed that their visible-light activities were firstly increased with increasing amount of Cu(II). When the amount of Cu(II) exceeded 0.1%, the photocatalytic activity of Cu(II)-TiO₂ decreased. The results demonstrated that 0.1% is the optimal amount of grafted Cu(II) nanoclusters for Cu(II)-TiO₂. Notably, the photocatalytic activity Cu(II)-TiO₂ prepared under these conditions was markedly superior to that of TiO_{2-x}N_x, which is considered to be one of the most efficient visible-

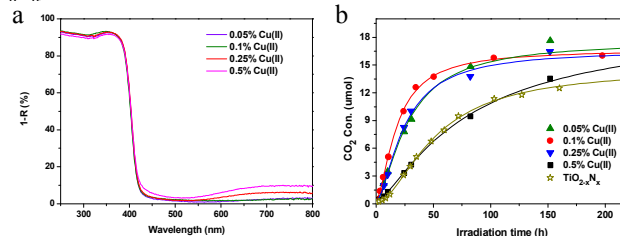


Figure 5 (a) UV-Vis spectra for Cu(II)-TiO₂ samples with different amounts of grafted Cu(II) at pH 12 and (b) photocatalytic activities of the Cu(II)-TiO₂ samples in (a) and N-doped TiO₂ under visible-light irradiation.

light photocatalysts.³² The calculated QE of the TiO_{2-x}N_x samples was only 3.9%, which is dramatically lower than that of our Cu(II)-TiO₂ (950-HCl-12) sample of 68.7% (Table 1).

3.2 Anti-viral activity of Cu(II)-TiO₂.

In addition to the photocatalytic property of TiO₂, the anti-bacterial and anti-viral properties of TiO₂ under light irradiation are also important for its practical applications.³³⁻³⁵ The photocatalytic inactivation of pathogenic microorganisms by Cu(II)-TiO₂ was evaluated using thin film samples that were prepared by coating suspensions of Cu(II)-TiO₂ (950-HCl-12) on glass substrates. Bacteriophage Q β was used as a model virus to measure the anti-viral activity of Cu(II)-TiO₂.²³ The anti-viral activity of the Cu(II)-TiO₂ nanocomposite was tested by the plaque assay according to the standard evaluation procedure for photocatalytic antiviral effect (Japanese Industrial Standards, JIS R1756). In the assay, test solutions containing bacteriophage Q β were used to infect *E. coli* (NBRC 13965), and the bacteriophage Q β concentration was determined from the number of PFU/mL.

As can be seen in Figure 6a, the Cu(II)-TiO₂ (950-HCl-7) sample exhibited only a negligible degree of bacteriophage inactivation in the dark, whereas obvious inactivation was observed under visible-light irradiation. Specifically, viral inactivation reached 99% and 99.99% under visible-light

Table 1 Summary of the photocatalytic performances of the Cu(II)-TiO₂ samples at different experimental conditions.

Experimental conditions	pH	Cu(II) amount	Initial photons (quanta/sec/cm ²)	Absorbed photons (quanta/sec/cm ²)	Reaction rate (μmol/h)	QE (%)
pH dependence	2	0.1%	1.3×10^{16}	4.43×10^{14}	0.07	15.8
	4	0.1%	1.3×10^{16}	4.53×10^{14}	0.10	22.1
	7	0.1%	1.3×10^{16}	4.62×10^{14}	0.14	30.3
	10	0.1%	1.3×10^{16}	4.84×10^{14}	0.24	49.6
	12	0.1%	1.3×10^{16}	5.82×10^{14}	0.40	68.7
	14	0.1%	1.3×10^{16}	6.48×10^{14}	0.05	7.7
Cu(II) amount dependence	12	0.05%	1.3×10^{16}	4.98×10^{14}	0.32	64.2
	12	0.25%	1.3×10^{16}	7.94×10^{14}	0.33	41.6
	12	0.5%	1.3×10^{16}	9.55×10^{14}	0.13	13.6

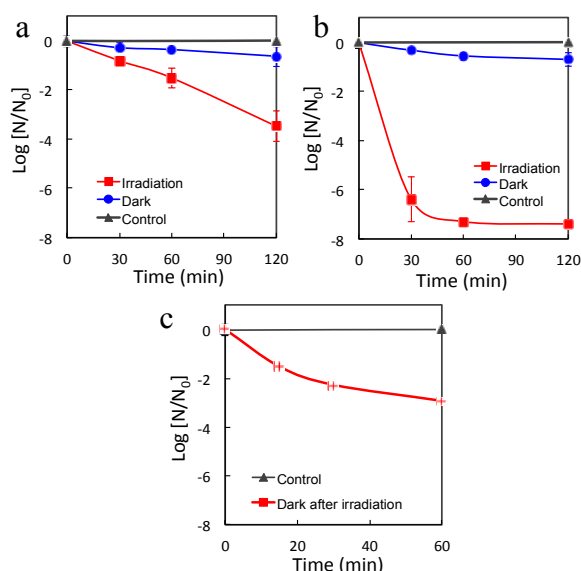


Figure 6. Inactivation of Q β bacteriophage by a) Cu(II)-TiO₂ (950-HCl-7) and b) Cu(II)-TiO₂ (950-HCl-12) under dark conditions and visible-light irradiation, and by c) Cu(II)-TiO₂ (950-HCl-12) under dark conditions after pre-irradiation treatment with visible-light.

irradiation for 1 and 2 h, respectively. Notably, the Cu(II)-TiO₂ (950-HCl-12) displayed a log₁₀(6.5) reduction of bacteriophage after only 30 min of visible-light irradiation (Figure 6b). This bacteriophage inactivation performance was identical to that of our previously reported Cu_xO/TiO₂ samples.²⁰ Figure 6c shows the effect of pre-irradiation treatment on the anti-viral activity of the Cu(II)-TiO₂ (950-HCl-12) sample under dark conditions. After 1 h of visible light pre-irradiation treatment, followed by a 1-h incubation under dark conditions, 99.9% of viral particles were inactivated. The anti-viral performance of Cu(II)-TiO₂ (950-HCl-12) under dark conditions was superior to that of Cu(II)-TiO₂ (950-HCl-7, Figure 6a) and conventional Cu(II)-TiO₂ (950-7) samples under visible-light irradiation,²⁰ as only two orders (99%) of virus were inactivated by the Cu(II)-TiO₂ samples during visible-

light irradiation for 1 h. As shown in Figure 6b, the Cu(II)-TiO₂ (950-HCl-12) sample only exhibited low anti-viral activity under dark conditions without irradiation treatment, confirming that the anti-viral activity of this photocatalytic material in the dark was attributable to the pre-irradiation treatment. Further, the anti-viral activity was directly influenced by the intensity of the light used for the pre-irradiation treatment. The sustained anti-viral activity of Cu(II)-TiO₂ (950-HCl-12) was enhanced when a strong visible-light source, such as a fluorescent lamp, or UV light source, such as a black light bulb, was used for the irradiation treatment (Figure S14).

The anti-bacterial and anti-viral properties of TiO₂ under light irradiation have been widely investigated^{33,34} and are attributed to the direct oxidation of virus by photogenerated holes or reactive radical species, such as ·OH radical, O₂⁻ and H₂O₂.³⁵ However, the inactivation speed of bacteria and virus on TiO₂ was limited by the step of disordering the outer membranes of bacteria and virus.³³ The anti-viral effects of Cu metal, Cu oxides, and Cu(II) ions have also been determined.^{23,36} The anti-viral effects on Cu species is attributed to the blocking of functional groups of proteins and inactivation of enzymes.²³ Our recent study demonstrated that Cu(I) species in Cu nanoclusters are much more effective than Cu metals or Cu(II) species for enhancing the anti-viral and anti-bacterial effects of TiO₂ photocatalysts.²⁰ Irie et al.¹⁹ investigated the role of Cu(II) nanoclusters in electron-trapping by in situ X-ray absorption fine structure (XAFS) analysis under visible-light irradiation in the presence of IPA and absence of oxygen and found that Cu(I) was generated under these conditions. Therefore, the presently observed anti-viral activity of Cu(II)-TiO₂ (950-HCl-12) under dark conditions after visible-light irradiation was induced by the Cu(I) species in the solid-state Cu(II) nanoclusters. Previous studies have demonstrated that the combination of TiO₂ with CuO or Cu₂O resulted in visible-light absorption and electron trapping among TiO₂ and these copper oxides under visible-light irradiation.^{37,38} The trapped electrons lead to the formation of highly reduced states of TiO₂/Cu(I) species, which are highly stable, even under

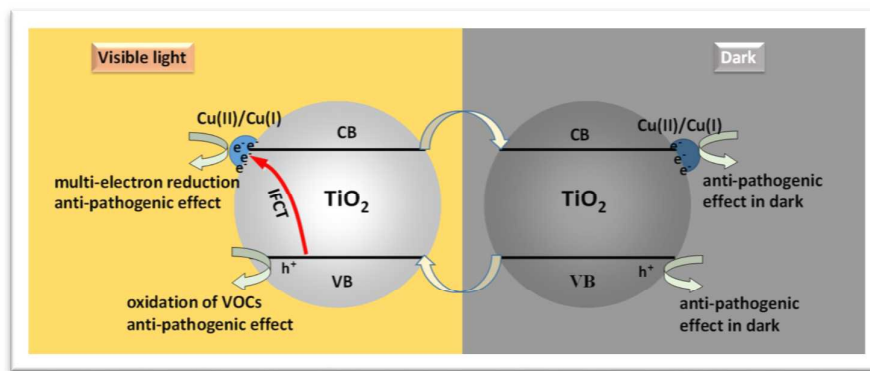


Figure 7. Proposed processes of photocatalysis and inactivation of viruses and bacteria under visible-light irradiation and dark conditions.

oxygen-saturated conditions, at the interface between TiO_2 and Cu(II) species.³⁹⁻⁴¹ The photogenerated electrons are trapped and stored in metal oxide semiconductors as donors and are gradually oxidized in air under dark conditions.³⁷⁻⁴¹

Figure 7 shows the possible mechanism underlying the sustained anti-viral activity of our photocatalyst in the absence of light irradiation. Under visible-light irradiation, electrons in the VB of TiO_2 are excited to the surface Cu(II) nanoclusters in a process that represents a form of IFCT and results in the transformation of Cu(II) into Cu(I) , with holes remaining in the VB. The generated Cu(I) can efficiently reduce oxygen molecules *via* a multi-electron reduction process that regenerates Cu(II) .¹⁴⁻¹⁶ The holes generated in the VB of TiO_2 possess strong oxidation power to decompose VOCs, a property that explains the high photooxidation activity of the TiO_2 (950-HCl-12) nanocomposites for IPA decomposition under visible-light irradiation. In addition, it has been demonstrated that Cu(I) species are very effective for enhancing the anti-viral and anti-bacterial effects of TiO_2 photocatalysts even under dark condition.²⁰ Following irradiation with visible light, holes generated in the VB of TiO_2 , in combination with Cu(I) species, can also attack the outer membrane, proteins, and nucleic acid (DNA and RNA) of viruses and bacteria, resulting in their death and inactivation.²⁰ Therefore, the obtained TiO_2 (950-HCl-12) nanocomposites exhibited a marked activity for anti-bacteria and antiviral under visible light irradiation. For the sustainability of antiviral activity under dark condition, remained Cu(I) species play an important role. It has been reported that the combination of TiO_2 with copper oxides, such as CuO or Cu_2O , not only resulted in visible-light absorption but also electron trapping in the interfaces among TiO_2 and these copper oxides under visible-light irradiation.^{37,38} Trapped electrons in Cu^{2+} species as Cu^{1+} states are thermodynamically more stable than those in the conduction band (CB) of TiO_2 ,^{37,38} since the redox potential of $\text{Cu}^{2+}/\text{Cu}^+$ in the Cu(II) nanoclusters is more positive than the CB of TiO_2 . Thus, a part of electrons could be trapped in Cu(II) nanoclusters near the interfaces, resulting the prevention of

recombination with holes in the VB.⁴² These trapped electrons in Cu(II) nanoclusters as Cu^{1+} species contribute to the sustained anti-bacterial and anti-viral properties under the dark condition. Moreover, the photocatalytic activity of the TiO_2 (950-HCl-12) sample was stable in air with a turnover number of greater than 60. These results indicate that both the photocatalytic VOC decomposition and anti-pathogenic effects of our synthesized Cu(II)-TiO_2 (950-HCl-12) nanocomposites can be sustained for long-term operation in indoor environments. These properties suggest that Cu(II)-TiO_2 (950-HCl-12) is a promising material for indoor environmental risk-reduction applications.

4. CONCLUSION

In summary, we succeeded in preparing highly visible-light-active Cu(II)-TiO_2 nanocomposites with sustained anti-viral properties through comprehensive optimization of the synthesis conditions, such as pre-annealing treatment of bare TiO_2 powder, washing treatment of TiO_2 in aqueous acid condition, and pH and amount of grafted Cu(II) nanoclusters. By optimizing the crystallinity, interfacial junction between TiO_2 and Cu(II) nanoclusters, and amount of Cu(II) nanoclusters, the synthesized Cu(II)-TiO_2 nanocomposites exhibited efficient IFCT and reductive energy storage properties. Thus, the photocatalytic nanocomposites efficiently decomposed VOCs and had strong antipathogenic effects in indoor conditions. Notably, the nanocomposites displayed sustained anti-viral activity in dark conditions after light irradiation. Based on these properties, our Cu(II)-TiO_2 nanocomposites are promising materials for risk-reduction applications in indoor environments. In addition, the synthesis approach described here represents a fundamental route to develop efficient nanocomposites for numerous target applications.

Acknowledgements

This work was performed under the management of the Project to Create Photocatalysts Industry for Recycling-Oriented Society supported by the New Energy and Industrial Technology Development Organization (NEDO) in Japan. This research was also supported by the ACT-C program of the Japan Science and Technology (JST) Agency.

References

- 1 J. D. Spengler, K. Sexton, *Science* 1983, **221**, 9–17.
- 2 N. E. Klepeis, W. C. Nelson, W. R. Ott, J. P. Robinson, A. M. Tsang, P. Switzer, J. V. Behar, S. C. Hern, W. H. Engelmann, *J. Expo. Anal. Environ. Epidemiol.* 2001, **11**, 231–252.
- 3 K. Harada, A. Hasegawa, C. N. Wei, K. Minamoto, Y. N. Noguchi, K. Hara, O. Matsushita, K. Noda, A. Ueda, *J. Health Sci.* 2010, **56**, 488–501.
- 4 D. M. Morens, G. K. Folkers, A. S. Fauci, *Nature* 2004, **430**, 242–249.
- 5 K. E. Jones, N. G. Patel, M. A. Levy, A. Storeygard, D. Balk, J. L. Gittleman, P. Daszak, *Nature* 2008, **451**, 990–993.
- 6 A. Fujishima, X. Zhang, A. D. Tryk, *Surf. Sci. Rep.* 2008, **63**, 515–582.
- 7 M. R. Hoffmann, S. T. Martin, W. Choi, D. W. Bahnemann, *Chem. Rev.* 1995, **95**, 69–96.
- 8 A. L. Linsebigler, G. Q. Lu, J. T. Yates, *Chem. Rev.* 1995, **95**, 735–758.
- 9 K. Hashimoto, H. Irie, A. Fujishima, *Jpn. J. Appl. Phys.* 2005, **44**, 8269–8285.
- 10 M. Miyauchi, A. Nakajima, K. Hashimoto, T. Watanabe, *Adv. Mater.* 2000, **12**, 1923–1927.
- 11 W. Y. Choi, A. Termin, M. R. Hoffmann, *J. Phys. Chem.* 1994, **98**, 13669–13679.
- 12 P. V. Kamat, D. Meisel, *Curr. Opin. Colloid Interface Sci.* 2002, **7**, 282–287.
- 13 H. Irie, Y. Watanabe, K. Hashimoto, *J. Phys. Chem. B* 2003, **107**, 5483–5486.
- 14 H. Irie, S. Miura, K. Kamiya, K. Hashimoto, *Chem. Phys. Lett.* 2008, **457**, 202–205.
- 15 H. G. Yu, H. Irie, K. Hashimoto, *J. Am. Chem. Soc.* 2010, **132**, 6898–6899.
- 16 H. G. Yu, H. Irie, Y. Shimodaira, Y. Hosogi, Y. Kuroda, M. Miyauchi, K. Hashimoto, *J. Phys. Chem. C* 2010, **114**, 16481–16487.
- 17 M. Liu, X. Q. Qiu, M. Miyauchi, K. Hashimoto, *Chem. Mater.* 2011, **23**, 5282–5286.
- 18 M. Liu, X. Q. Qiu, M. Miyauchi, K. Hashimoto, *J. Am. Chem. Soc.* 2013, **135**, 10064–10072.
- 19 H. Irie, K. Kamiya, T. Shibamura, S. Miura, D. A. Trky, T. Yokoyama, K. Hashimoto, *J. Phys. Chem. C* 2009, **113**, 10761–10766.
- 20 X. Q. Qiu, M. Miyauchi, K. Sunada, M. Minoshima, M. Liu, Y. Lu, D. Li, Y. Shimodaira, Y. Hosogi, Y. Kuroda, K. Hashimoto, *ACS Nano* 2012, **6**, 1609–1618.
- 21 M. Liu, X. Q. Qiu, M. Miyauchi, K. Hashimoto, *J. Mater. Chem. A* 2014, **2**, 13571–13579.
- 22 M. Liu, R. Inde, M. Nishikawa, X. Q. Qiu, D. Atarashi, E. Sakai, Y. Nosaka, K. Hashimoto, M. Miyauchi, *ACS Nano* 2014, **8**, 7229–7238.
- 23 K. Sunada, M. Minoshima, K. Hashimoto, *J. Hazard. Mater.* 2012, **235-236**, 265–270.
- 24 S. Brunauer, P. H. Emmett and E. Teller, *J. Am. Chem. Soc.* 1938, **60**, 309–319.
- 25 A. S. Attar, M. S. Ghamsari, F. Hajiesmaeilbaigi, S. Mirdamadi, K. Katagiri, K. Koumoto, *J. Mater. Sci.* 2008, **43**, 5924–5929.
- 26 B. D. Cullity, S. R. Stock, *Elements of X-Ray Diffraction*, 3rd ed.; Prentice-Hall Inc.: Upper Saddle River, NJ, 2001.
- 27 P. Wolkoff, G. D. Nielsen, *Atmos. Environ.* 2001, **35**, 4407–4417.
- 28 Y. Ohko, K. Hashimoto, A. Fujishima, *J. Phys. Chem. A* 1997, **101**, 8057–8062.
- 29 H. G. Yu, J. G. Yu, B. Cheng, *Catal. Commun.* 2006, **7**, 1000–1004.
- 30 J. G. Yu, X. J. Zhao, *Mater. Res. Bull.* 2000, **35**, 1293–1301.
- 31 F. Boccuzzi, A. Chiorino, G. Martra, M. Gargano, N. Ravasio, B. Carrozzini, *J. Catal.* 1997, **165**, 129–139.
- 32 R. Asahi, T. Morikawa, T. Ohwaki, K. Aoki, Y. Taga, *Science* 2001, **293**, 269–271.
- 33 M. Cho, H. M. Chung, W. Y. Choi, J. Y. Yoon, *Appl. Environ. Microbiol.* 2005, **71**, 270–275.
- 34 K. Sunada, T. Watanabe, K. Hashimoto, *J. Photochem. Photobiol. A* 2003, **156**, 227–233.
- 35 T. Watanabe, A. Kitamura, E. Kojima, C. Nakayama, K. Hashimoto, A. Fujishima, *Photocatalytic Purification and Treatment of Water and Air*, Elsevier, New York, 1993, 747–751.
- 36 J. L. Sagripanti, L. B. Routson, C. D. Lytle, *Appl. Environ. Microbiol.* 1993, **59**, 4374–4376.
- 37 J. Bandara, C. P. K. Udawatta, C. S. K. Rajapakse, *Photochem. Photobiol. Sci.* 2005, **4**, 857–861.
- 38 J. P. Yasomanee, J. Bandara, *Sol. Energy Mater. Sol. Cells* 2008, **92**, 348–352.
- 39 T. Tatsuma, S. Saitoh, Y. Ohko, A. Fujishima, *Chem. Mater.* 2001, **13**, 2838–2842.
- 40 T. Tatsuma, S. Saitoh, Y. Ohko, A. Fujishima, *Electrochemistry* 2002, **70**, 460–462.
- 41 T. Tatsuma, S. Saitoh, P. Ngaotrakanwivat, Y. Ohko, A. Fujishima, *Langmuir* 2002, **18**, 7777–7779.
- 42 J. Li, Y. Liu, Z. J. Zhu, G. Z. Zhang, T. Zou, Z. J. Zou, S. P. Zhang, D. W. Zeng, and C. S. Xie, *Sci. Rep.* 2013, **3**, 2049.

Table of Contents Graphic

